

# Fluid-Structure Interactions: Research in the Courant Institute's Applied Mathematics Laboratory

STEPHEN CHILDRESS

*Courant Institute*

MICHAEL SHELLEY

*Courant Institute*

AND

JUN ZHANG

*Courant Institute*

*Department of Physics, New York University*

## Abstract

The Applied Mathematics Laboratory is a research laboratory within the Mathematics Department of the Courant Institute. It was established to carry out physical experiments, modeling, and associated numerical studies in a variety of problems of interest to Courant faculty, postdocs, and graduate and undergraduate students. Most of the research to date has involved fluid mechanics, and we focus in this paper on the work that relates to the interaction of fluids with rigid, movable, or flexible bodies. © 2012 Wiley Periodicals, Inc.

## 1 Introduction: A Brief History of the AML

Although the Courant Institute has a long and notable history of applied mathematics research, until the late 1990s this work had been almost entirely theoretical. One notable exception is captured in a photograph, reproduced in Figure 1.1, of Richard Courant illustrating a minimal surface by suspending soap film from a wire frame. While fluid dynamics was not the point here, the viewers may well have noted the beautiful flows of material that can be seen within such films as the fluid drains and redistributes itself. Fifty years later applications using soap films reappeared at the Institute in the Applied Mathematics Laboratory, or AML, though now to study complex fluid dynamical phenomena involving the interaction of bodies with high-speed fluid flows.

The Applied Math Lab is an experimental research laboratory within the Institute. The research interests of the lab are broad but our primary work is in the dynamics of fluids. We shall focus here on one particular area of interest to us in recent years, namely, fluid-structure interactions. A beautiful example is shown

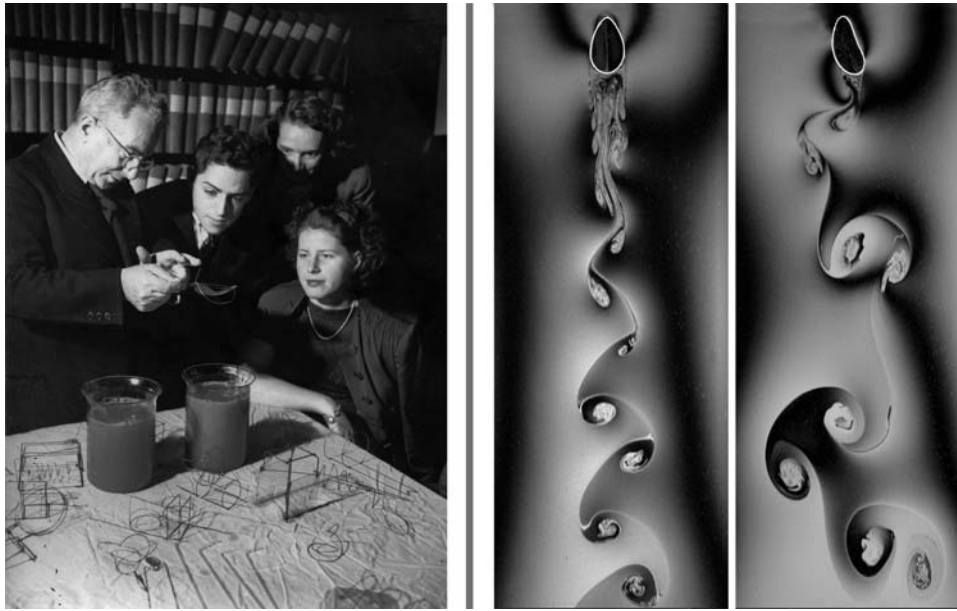


FIGURE 1.1. Richard Courant (left) using a suspended soap film to illustrate minimal surfaces, circa 1946. Reproduced with permission of the Courant Institute, New York University. Right: In a flowing soap film, the wakes swept below a flexible loop embedded within the film [21]. The coupled fluid-structure system shows bistability, with a stationary state and an oscillatory state. Reproduced with permission of the authors.

in Figure 1.1. A deformable loop—a two-dimensional balloon—interacts with an oncoming flow and sheds vortical structures downstream.

In this introduction, we give a very brief history of the AML. There is some tradition for having experimental labs in mathematics environments. The longstanding fluids labs at DAMTP in Cambridge University, in the Applied Mathematics Department at MIT, and in Mathematics at Penn State are three examples. More recent laboratories are now in place at Arizona, Delaware, UCLA, and UNC. The Courant Institute’s AML—originally called the WetLab—was founded in 1996 by Childress and Shelley as a combined experimental and computational facility. The impetus for its founding was the lack of experimental research in fluid dynamics in our New York City neighborhood, and the conviction that the best applied mathematics and simulation were tied to real applications and interesting experiments. We sought to reinforce this notion by having our own lab combine the equipment of experiment with the equipment of theory, which is the computer.

The AML at first consisted of one large lab room, and an adjacent computer lab stocked with Silicon Graphics computers that were generously donated by SGI Inc. The overall space was created from a suite of offices on the ground floor

of Warren Weaver Hall that were gutted and renovated to create usable lab space using support from a bequest by the William A. Sears family to NYU and from the Mobil Foundation. The Institute's director at that time, David McLaughlin, was very supportive in securing the funds and the space, and later in securing an associated faculty position. SC and MS lent a hand to the AML's design by setting its electrical power outlets into the floor where, with gravity's help, fluids could easily drain (these were later sealed and electricity accessed through drop-downs from the ceiling).

Our clear need for an actual experimentalist in the lab was met with the assistance of Albert Libchaber's biophysics lab at Rockefeller University. SC had then for been working with Libchaber and one of his postdocs, Jun Zhang, on an experiment of thermal convection at high Rayleigh number [55, 56]. Soon afterward Jun agreed to work part-time in the AML, which he outfitted with basic equipment and tools. Soon thereafter he became a full-time postdoc in the lab, and following that he accepted a joint appointment in the faculties of Physics and Mathematics at NYU and is now one of the AML's directors.

Simultaneously, the infrastructure of the AML began to evolve. Computing had become progressively delocalized and the need for dedicated computer labs had waned. At the same time, the need for more experimental space in the AML became apparent and the computer lab was converted into more experimental lab space.

The first thermal convection experiments eventually led to a set of experiments that investigated how convecting fluids, such as the Earth's mantle, interact with movable objects, like the Earth's continents. The observed dynamics is related to the so-called Wilson cycle of continental drift. Additional experiments on fluid-structure interactions concerned the flapping of flags in fluid flows and were inspired by the swimming of fish. Biology and locomotion have been a constant motivation for work in the AML, and the flag experiment has led to other experiments, concerning, for example, drag reduction by flexible bodies bending in a flow, the mechanisms of flapping flight, hovering, and valveless pumping. Developing areas of research in the AML concern collective behavior, pattern formation in geophysics, and the dynamics of complex and active fluids. These experiments are discussed in detail below. We also touch upon the many accompanying theoretical and numerical studies that interacted with and informed the experiments.

## 2 Fluid-Structure Interactions in Soap-Film Flows

One of the first experimental devices built in the AML was a *soap-film flow tunnel*, an elegant apparatus that had been developed in other laboratories to study laminar and turbulent two-dimensional fluid flows [12, 16, 34]. Two stretches of nylon fishing line emanate downward from an upper reservoir of soap solution. By separating the lines a gravity-driven flowing film is formed between them. In our flow tunnel the width of the film is about 10 cm and the range of gravity-driven flow speeds is 0.5–3 m/s. The patterns of flow in the film cause slight changes

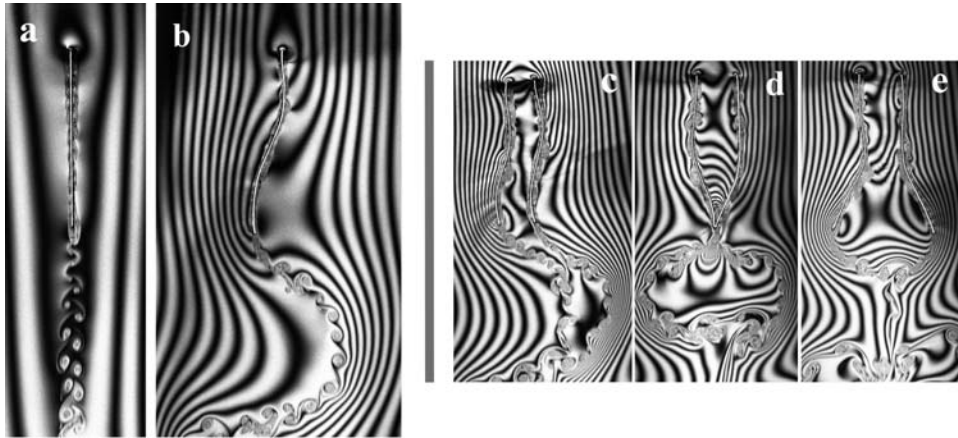


FIGURE 2.1. Left panel: The (a) stretched-straight and (b) flapping states of a “flag” in a quasi-two-dimensional flow of a soap film. Here the dynamics is in the bistable regime. Right panel: The (c) in-phase and (d, e) out-of-phase states of two nearby flags. Reproduced from [57] with permission of the authors.

in its thickness, which can be visualized using interference fringes from reflected sodium light. Figure 1.1 illustrates how these fringes reveal the vortical structures in the flow, and also shows that a flowing soap film can be used to investigate the interactions between high-speed flows and flexible bodies.

## 2.1 Flapping of Flags

In particular, the flapping of a flag is amenable to study in this flow device. To do this, a short length of flexible thread (2–6 cm) is wetted into the film and fixed at one end, so that it is stretched out by the flow. While the film is very thin compared to the thread— $\sim 4 \mu\text{m}$  versus  $150 \mu\text{m}$ —it also flows very fast and so can apply appreciable fluid forces. Given the setting, this experiment essentially investigates the dynamics of a one-dimensional flag in a two-dimensional flow; see Zhang et al. [57].

Figure 2.1(a) shows two examples of the flow pattern. We find that if the “flag” is short, its stable position is simply stretched straight (SS), with a thin von Kármán wake shed downstream as seen in (a). However, by slowly increasing the length, we find that there is a critical length beyond which the SS-state is not stable, and the flag instead “flaps,” through traveling waves of deformation moving from head to tail, as seen in Figure 2.1(b). The wake structure also changes: on each half-stroke the flag sheds vortex layers of alternating sign with local Kelvin-Helmholtz instabilities developing along them. Surprisingly, this bifurcation is hysteretic. Decreasing the flag length yields flapping to a second critical length, smaller than the first, below which the SS state reappears. Between these two critical lengths there is a range of bistability where the flapping and SS states coexist as stable states.

These results were not in accord with the classical understanding of the flapping of flags. Theoretical treatments originate with Lord Rayleigh [32], whose theory is a special degenerate case of the Rayleigh-Helmholtz instability. The latter considers a parallel flow between two regions of fluid having equal velocity and density. The two fluids are allowed to slip at a dividing interface. A slight distortion in the interface away from being flat produces a discontinuity in the velocity at the interface, and the interface is then a vortex sheet which, in Rayleigh's conception, corresponds to the flag. Here the surface vorticity thus produced is *free* and moves downstream in the flow. A sinusoidal vorticity variation produces steady lateral migration of fluid particles, and the lateral displacement of the virtual interface, or flag, grows linearly with distance downstream.

While Rayleigh's model captures important features of the physics, it is incomplete and not in accord with experimental results. In particular, Rayleigh's model does not account for the materiality of the flag: the interface lacks its own inertia, as well as internal mechanics such as bending and tensile forces. Lacking these elements, Rayleigh's model predicts that any perturbation, no matter how small, will lead to instability. This is not in accord with the existence of the SS state. Rayleigh's model is actually most appropriate to describing the wake shed by the flag, where the vorticity produced in the boundary layers along the flag has been shed, and which moves freely downstream.

In counterpoint, our laboratory flag exhibits the essential elements of fluid-structure interaction, in that the mass of the flag and its elastic properties are essential to understanding the dynamics, properties which tend to be obscured for large cloth flags subject to gravity. Alben and Shelley developed a fully nonlinear two-dimensional elaboration of Rayleigh's vortex sheet model that accounts for these elements, as well as the shedding of vorticity off the flag into a free wake [2, 5]. Stability analyses and nonlinear simulations of this model predict a linear instability dependent upon flag mass, which is consistent with experiment, and the existence of the bistable state [1, 5, 39]. Other experiments using the AML's water tunnel showed that to flap in flowing water, flags needed to be much heavier. These special flags were constructed of parallel metal panels glued to a flexible substrate [39]. These various experiments motivated other experimental and simulation studies that were recently reviewed by Shelley and Zhang [40]. We would like to especially note those done by our colleague Charles Peskin and his students using new versions of the immersed boundary method that account for flag mass [22, 61].

If *two* identical flags are placed side by side in the soap film, a state of flapping in or out of phase with each other can occur along with the stretched-straight state; see Figure 2.1(c,d,e). Flags sufficiently far apart behave independently, but as the separation distance is reduced below about half the flag length, these three different states are observed, with in-phase flapping occurring as the separation becomes sufficiently small. Numerical studies using the immersed boundary method [60] and the nonlinear vortex sheet model [3] have since reproduced these dynamics.

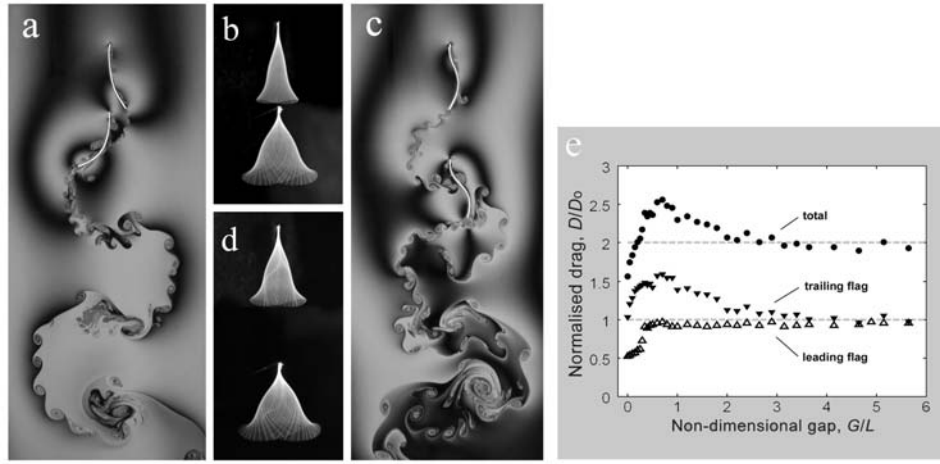


FIGURE 2.2. A pair of tandem flags flap in a downward flowing soap film at two different separations. (a) and (c) show visualization by thin-film interferometry, while (b) and (d) are their respective visualizations as long-time exposure photographs. Panel (e) shows the normalized fluid drag on the tandem flags as a function of separation distance. Reproduced from [33] with permission of the authors.

## 2.2 Drafting of Flexible Bodies

The flapping motion of our flags bears a close resemblance to the movements of a steadily swimming fish, and it has been argued that fish movements are largely a natural response of a slender, massive, elastic object to an ambient flow [25]. In this view, the additional movements needed to generate the required thrust are small modifications of a basic flapping mode. It is also of interest to further compare the flapping states of multiple flags with the observed, coordinated movements of schools of fish.

The fish-flag paradigm suggests another experiment related to the energetics of schooling fish [54]. If two identical objects are placed one behind the other in a steady flow, it is customary to think of the leading body as experiencing the higher drag (drafting effect) of the two. Indeed this is observed in experiments and is exploited by racing cyclists and race car drivers. But do fish draft?

To approach this problem, we put in tandem two identical flags and measured the drag forces on each; see Figure 2.2. Much to our surprise we found that the trailing flag had increased drag relative to the single flag case while the leading flag had smaller [33]. For a group of six flags placed in tandem, the leading flag again had smaller drag than the second flag. A partial explanation of this result lies in the interaction of the flapping dynamic of the second flag with the vortical wake created by the first flag and in the impedance to tail flapping of the first flag provided by its proximity to the second. This case of inverted drafting need not

be applicable to a thrust-generating pair of fish, but it illustrates the complexity of flow interactions that can occur between multiple flexible bodies.

### 2.3 Self-Streamlining of Flexible Bodies

The flapping instability of flags aligned with a flow is produced by growth of traveling waves. A very different problem concerns the bending of flexible bodies that instead obstruct a flow. Obstructing and bending under flow is part of the life of sessile organisms such as trees [29], coral, and seaweeds [24, 44]. Indeed, the reconfiguration of elastically flexible bodies by fluid flows is common in nature and can yield substantial and beneficial drag reduction [13, 23]. A particularly elegant example is given by S. Vogel [52], who studied the shape reconfiguration of tree leaves when placed in a wind tunnel. He observed that as wind speed increased, the leaves rolled themselves into ever tighter cones, a self-streamlining mediated by body flexibility that yielded a drag growth slower than the classical rigid-body  $U^2$  law.

These observations motivated a study of self-streamlining in a simpler and more controlled setting (see Alben, Shelley, and Zhang [6, 7]). Using again a soap film tunnel we considered the bending of a flexible fiber (here a length of fiber optic glass) held transverse to the oncoming flow. This is a one-dimensional leaf in a two-dimensional wind; see Figure 2.3. At low flow speeds (panel (a)), the fiber remains nearly straight, and from its ends are shed sharp shear layers. The wake extends downstream, is roughly symmetric, and is very slowly moving relative to the outer flow. As flow speed increases (panels (b) and (c)) the fiber becomes more bent and streamlined. As a function of flow speed and other parameters, the drag on the fiber, the fiber shape, and the wake structure were all recorded simultaneously, with Reynolds numbers ranging from 2000 to 40,000. From these experiments and an associated theory, we hoped to discover an exponent  $\alpha$  that corrected the classical drag law to  $U^{2-\alpha}$  and thus accounted for velocity-dependent shape change.

Looking at steady-state behavior, we modeled this system using a generalization of free-streamline theory [17, 19] to construct simple steady flows around surfaces whose shapes were given by the balance of bending, tensile, and fluid pressure forces. After normalization, the system retains a single control parameter  $\eta$ , which is essentially a nondimensional flow velocity,

$$\eta = \left( \frac{\rho f L^3 U^2 / 2}{E} \right)^{1/2},$$

where  $\rho$  is fluid density,  $L$  is the fiber length,  $f$  is soap film thickness,  $U$  the free-stream velocity, and  $E$  the fiber flexural rigidity. Further note that  $\eta$  can be expressed as the ratio of fiber length  $L$  to an intrinsic length  $L_0$ :  $\eta = (L/L_0)^{3/2}$  where  $L_0 = (2E/\rho f U^2)^{1/3}$ . If this intrinsic length, which scales as  $U^{-2/3}$ , defines the effective cross section of the body to the flow, we then expect that at large velocities the fluid drag on this deformable body to scale as  $U^{2-2/3} = U^{4/3}$ , and

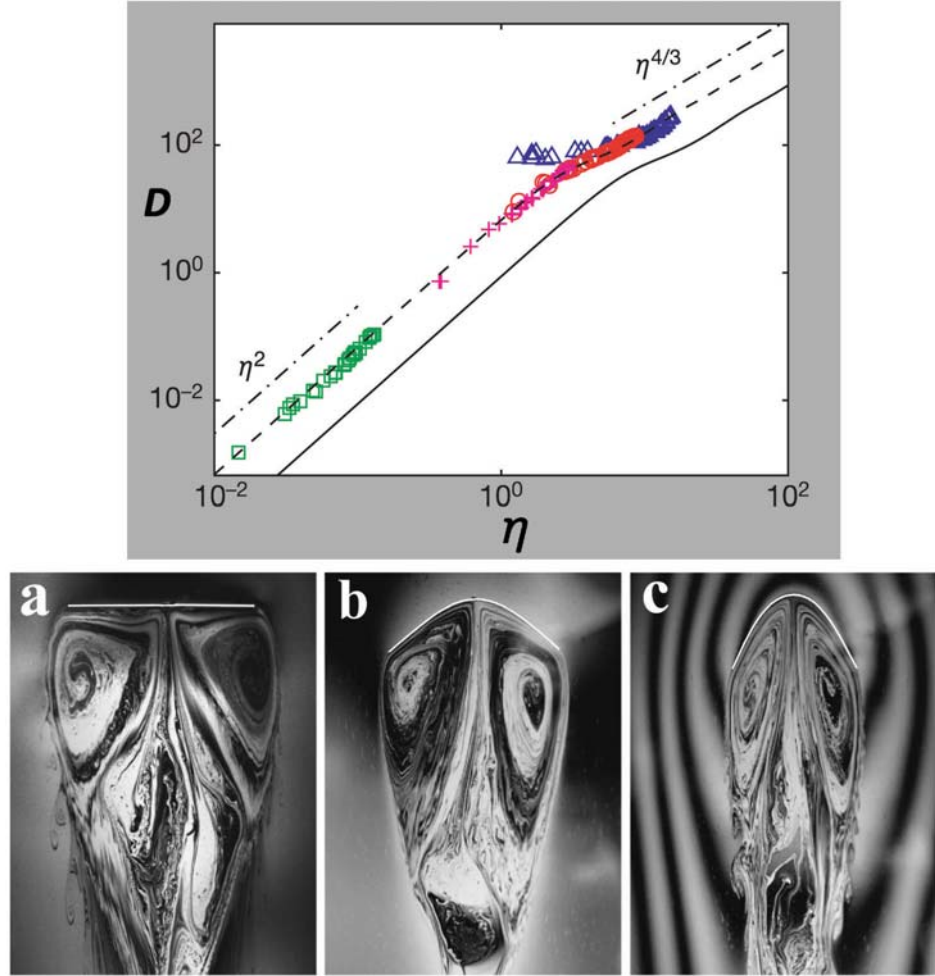


FIGURE 2.3. Top panel: From [6, 7], normalized experimental drag data (symbols) and theoretical drag relation (solid), as a function of the dimensionless flow velocity  $\eta$ . Dot-dash lines correspond to drag laws of  $\eta^2$  and  $\eta^{4/3}$ . Bottom panel: Fibers in the soap film shown with interferometry. (a) Flow past a rigid fiber. Flows around a flexible fiber at flow speeds of (b) 69 cm/s and (c) 144 cm/s. Reproduced from [6, 7] with permission of the authors.

hence  $\alpha = \frac{2}{3}$ . This prediction is consistent with our experimental data. Figure 2.3 (top) shows the measured drag plotted as a function of normalized velocity  $\eta$ . The drag for small  $\eta$  grows as  $\eta^2$  and then transits at  $\eta \sim O(1)$  to a new growth law, presumably  $\eta^{4/3}$ .

In the accompanying theoretical study [6, 7], we showed the close concordance between shapes computed from our theory and those measured experimentally. We showed also that the new  $\eta^{4/3}$  drag law was associated with the emergence of shape self-similarity at large  $\eta$  and gave an asymptotic construction of these shapes.

### 3 Self-Organization of Bodies in Thermal Convection

Thermal convection is ubiquitous in nature and occurs on length scales ranging from millimeters to the planetary scales of thousands of kilometers. We are interested here in a particular aspect of convection involving an interaction between freely floating bodies and an underlying convection flow. The experiment is motivated by the facts of continental drift and plate tectonics. Convective processes within the Earth's mantle are believed to drive the movements of plates in the Earth's upper crust, but it is not so clear how the convection depends on the disposition of plates.

We decided to study this in a simple model system involving an insulating floater—the model “continent”—that sits above a viscous fluid undergoing thermal convection. Here the continent plays both an active role, since it can serve as a thermal blanket on the underlying “hot” fluid, and a passive one, since viscous stresses associated with the convection can change its position. Our experimental system overlooks many of the geophysical details but retains three features that are of vital importance to the feedback process: (1) The range of the Rayleigh number (the principal measure of convective intensity and state) of our tabletop experiments covers that relevant to mantle convection,  $Ra \sim 10^7$ ; (2) the thermal blanket effect of the continents—heat loss through the continents is about only one-tenth of that through the oceanic crust—is reproduced; and (3) the motion of the continents to the movement and deformations of the underlying mantle as a viscous fluid adhering to and exerting viscous stress on the continent.

In our early experiments [58], a single continent is introduced onto the free surface of a convection cell; see Figure 3.1. The thermally opaque continent causes heat to accumulate below it, and the warm, buoyant fluid thus formed tends to rise, inducing an upwelling flow (top panel). In this way the continent modifies the flow pattern that drives its motion. As a consequence, the coupled system becomes unstable and the continent is moved to a new position at the other side of the cell (second panel). Such an action-reaction loop leads to an oscillation (bottom two panels). This oscillation is robust despite the fact that the thermal convection at this large Rayleigh number is highly turbulent, with the convecting fluid being filled with small-scale plumes. The likely root of this robustness is the persistence of a large-scale convective flow (see Childress [9]) and the model continent being large relative to the small-scale fluctuations.

We then asked the following question: if a large number of small continents are present in the convective system and each acts as a small thermal blanket, what will happen? To study this we immerse several hundred small spheres within the convecting fluid, and being somewhat more dense than the fluid, they settle to the

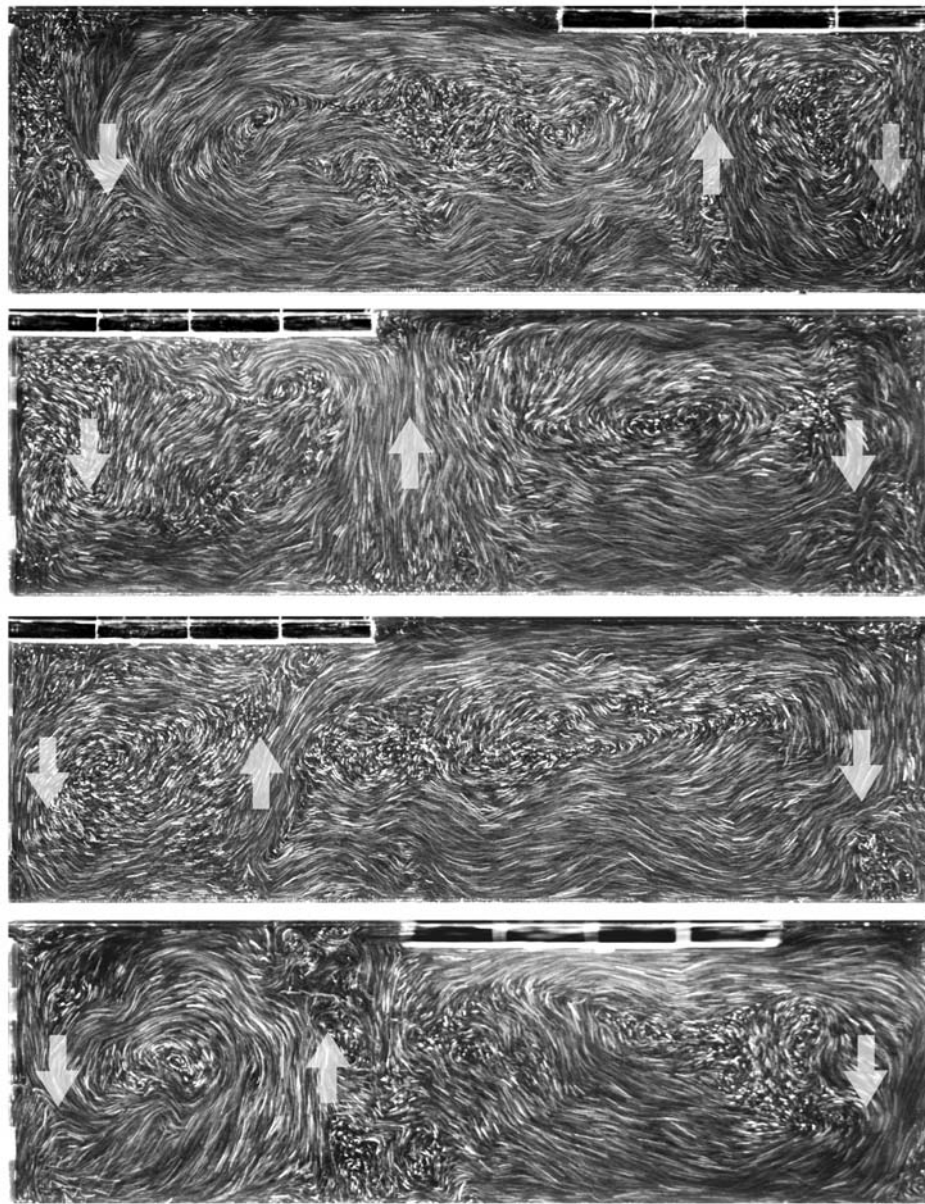


FIGURE 3.1. Visualization of thermally convective flow inside a fluid cell with a floating boundary. Here the boundary covers 40% of the upper fluid surface. We use illuminated liquid-crystal beads for visualizing the flow lines. (Top panel) Just before the free boundary is entrained toward the left; (second panel) after the floating boundary arrives at the left side of the cell; (third panel) shortly before the boundary starts to move back to the right; (bottom panel) while moving to the right. Reproduced with permission of the authors [59].

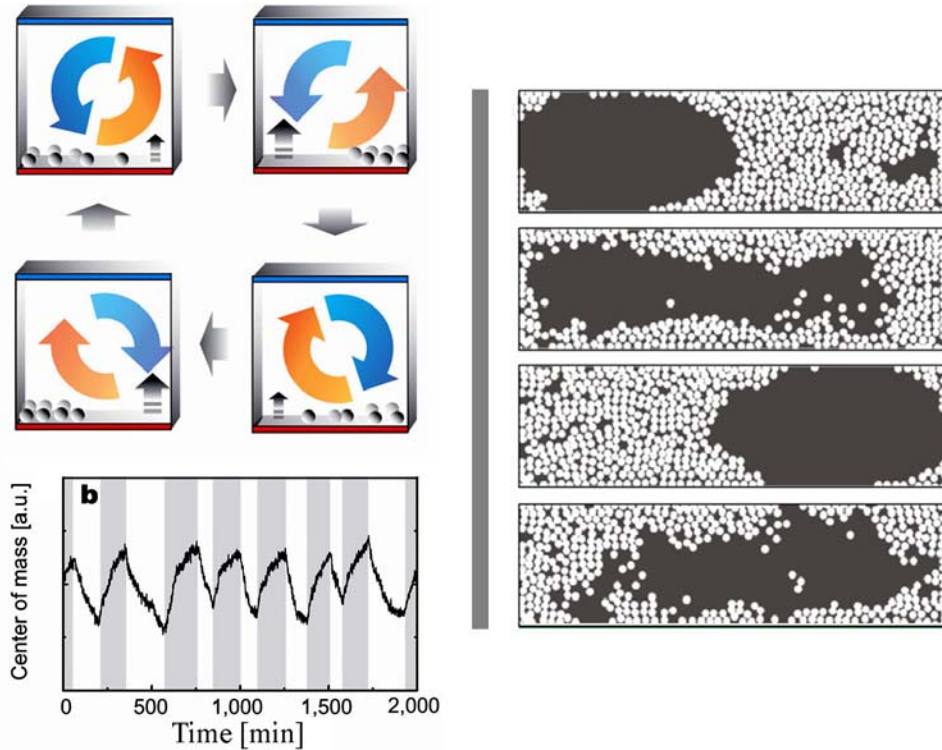


FIGURE 3.2. Thermal convection and free-moving bodies. Top left: The feedback mechanism is outlined in the top four panels, where thermal blanket effect of the spheres overturns the existing flow direction and the sphere are entrained by the flow. Right: Snapshots of hundreds of spheres undergoing collective oscillations as they interact with the convective fluid. Bottom left: Time series of the center of mass of the spheres, showing a cyclic oscillation. Reproduced from [27] with permission of the authors.

bottom (the blanketing effect now acts upon heat flux from the convecting cell's base). The dynamics of this system is illustrated in Figure 3.2. The outcome is surprising but quite simple. The mobile spheres aggregate into a single mass that executes the familiar oscillatory movements of our continent, though more as a condensed "gas" covering the bottom than as a solid. In our study (Liu and Zhang [27]) we determined the oscillation frequency as a function of sphere size, sphere number (coverage), and the Rayleigh number. Geophysical processes are complex but nonetheless obey simple physical laws. Studies such as these, by focusing on a few key elements, can provide insight into their underlying mechanisms.

## 4 Locomotion in Fluids

One of the most interesting and widely observed fluid-body interactions occurs in animal locomotion. A swimming fish, a flying bird, or an undulating flagellar microorganism is moving through the fluid while simultaneously reacting to the forces exerted by the fluid. All of the elements, illustrated by flag flapping, are generally present: there are time-dependent pressure and viscous forces that act on a time-dependent flexible object of given mass distribution. But in addition the locomoting animal is *free*, and so its rigid body motion (defined by establishing a suitable body frame) has to be determined along with the velocity and pressure fields of the fluid.

One important and somewhat counterintuitive fact about unaccelerated motion through a fluid is a simple consequence of Newton's second and third laws: if the organism is neutrally buoyant, the time-averaged force exerted by the body on the fluid and by the fluid on the body must vanish. Because of the nonlinearity of the Navier-Stokes equations, locomotion problems cannot in general be broken down into separate computations of thrust and drag. Also, since the steadily locomoting (constant velocity) body does no net work on the fluid, the efficiency of locomotion is not obviously quantifiable, and this has a bearing on attempts to optimize performance.

Because of these complexities, locomotion problems offer prime opportunities for physical and numerical experimentation. G. I. Taylor, in a famous experiment presented in one of the films produced by the National Committee for Fluid Mechanics [45], showed two basic strategies for swimming through a fluid. Simultaneously Taylor illustrated the importance of the *Reynolds number* in determining the effectiveness of a given swimming style. For our purposes the Reynolds number may be defined as  $Re = UL/\nu$  where  $U$  is the swimming velocity,  $L$  a body length, and  $\nu$  the kinematic viscosity of the fluid. One of Taylor's swimming devices consisted of a spherical head attached to a thin rubber tube. A spiral wire was inserted into the tube and turned by a rubber band mechanism within the head. When placed in thick syrup (large  $\nu$ , or small  $Re$ ), a helical wave moved down the model "flagellum" and the object swam just as a screw would be driven through a medium. The second swimmer was a body attached to a simple fin that flapped back and forth. Placed in water, this object swam (at large  $Re$ ) with a fishlike undulation. Taylor then reversed the fluids and the body equipped with the flagellum failed to move in water, and the flapper failed to move in syrup. The flapper in water exhibits swimming at large  $Re$ , the so-called Eulerian realm of locomotion. The flagellum in syrup swims at a small  $Re$  and represents the *Stokesian realm* of locomotion, where the Stokes approximation to the hydrodynamic equations applies. Each mechanism is adapted to the Reynolds number range at which it must operate and fails when well outside that range.

#### 4.1 Emergence of Locomotion by Active Flapping

To illustrate our work on locomotion in the AML, we first consider the question of transition between the two extremes represented by Taylor's experiment. The research to be described originated in studies by one of us (SC) at McMurdo Station, Antarctica, in collaboration with the biologist Robert Dudley, of the swimming of the “sea butterfly” *Clione antarctica*. This creature is a shell-less mollusk, which in its juvenile form is a small ( $\sim 0.5$  cm) cigar-shaped body equipped with three encircling rings of cilia. But it also has a pair of small wings tucked into forward pockets, which can be extended at will and made to beat up and down in a simple flapping motion.

Cilia, like flagella, are the appendages of choice for swimming in the Stokesian realm, while the wings are adapted to the Eulerian realm. It so happens that the Reynolds number of the young *Clione* was in the range  $10^1$ – $10^2$ , an intermediate range between Eulerian and Stokesian regimes, and so these organisms offered us the opportunity to study the relative advantages of cilium and wing as the organisms grew, increasing  $L$  and hence  $Re$ . Dudley was able, using small jets of water, to elicit swimming in two modes, either using the cilia or using the wings. Focusing on swimming using the wings, we may define a *frequency Reynolds number*  $Re_f = Lf^2/\nu$  where  $f$  is the frequency of flapping. When we plotted measurements of the swimming velocity in flapping mode, expressed through the Reynolds number  $Re$  as defined above, as a function of  $Re_f$ , we found that  $Re$  extrapolated to 0 at a finite value  $\sim 12$  for  $Re_f$  [10]. Our results thus suggested the existence of a mathematical bifurcation in swimming speed as a function of  $Re_f$ ; flapping “flight” ceased to be possible below a critical value  $Re_f^c \sim 12$ .

Such a conclusion is consistent with known results for Stokesian and Eulerian locomotion. In Stokes flow, the *scallop theorem* [31] is fundamental to understanding the mechanisms of locomotion. Stokes' approximation to the Navier-Stokes equations drops the acceleration terms. In incompressible flow we then have

$$\nabla p - \mu \nabla^2 \mathbf{u} = \mathbf{0}, \quad \nabla \cdot \mathbf{u} = 0,$$

where  $p$  and  $\mathbf{u}$  are the pressure and velocity fields and  $\mu$  is the fluid viscosity. Explicit time is thereby eliminated from the dynamics. Also, it is known that the exterior problem with prescribed  $\mathbf{u}$  can be solved uniquely, with the entire flow field being set up instantaneously by the boundary velocity (and the value of pressure at one point, e.g., infinity). As the body is deformed relative to a body frame, the associated rigid-body motion of the frame is determined by the instantaneous vanishing of force and torque. Suppose that the body motion is periodic relative to the body frame but is invariant under time reversal. The opening and closing of a scallop shell offers an example of such *reciprocal* motions. It then follows that the object cannot locomote, since forward and reverse rigid body movements agree. A simple up-and-down movement of a flapper is another example of a reciprocal motion, hence also one inoperative at zero  $Re$ . It is such a reciprocal motion that *Clione* uses in its flapping mode.

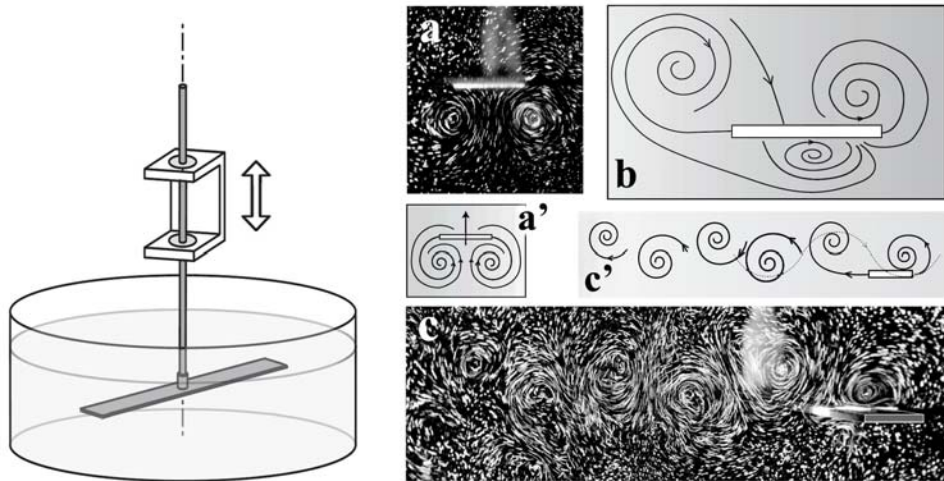


FIGURE 4.1. Left: Schematic of an experimental device to investigate free flapping flight. Right: Visualization of the flow structures around a flapping wing. (a) At low  $Re_f$  in its stable nonrotating state. (a') The direction of the wing motion and the flow structure corresponding to (a). (b) The flow structure associated with the accelerating wing. (c) The wake of the wing in the rotating state exhibits an ‘inverted’ von Kármán vortex street. (c') The direction of the flow and the motion of the wing (dashed line). Reproduced from [51] with permission of the authors.

On the other hand, the aerodynamics of flapping wings at large  $Re$  insures the production of thrust and therefore forward flapping flight. According to two-dimensional airfoil theory, the lift in steady flow is orthogonal to the oncoming stream. *Quasi-steady* flapping, defined by the inequality  $fL/U \ll 1$ , produces lift orthogonal to the *apparent* wind, and this is seen to imply a forward component of the ‘lift’ in both up and down strokes. Note that this lift-based thrust is obtained once the wing is actually in flight. Consequently, it is reasonable to assume that swimming or flight utilizing a simple reciprocal action of a wing becomes effective within an intermediate range of Reynolds numbers.

To test this idea in our laboratory we used the device shown in Figure 4.1. A stiff rectangular wing is attached at its center to a rod and is free to rotate. The rod is driven up and down in a tank of fluid. If the frequency is sufficiently small, we observe that the wing does not rotate, and if made to rotate it comes to a stop. Above a critical frequency, however, rotation of the wing ensues spontaneously, in a direction that is random; see Vandenberghe et al. [50, 51]. Thus locomotion occurs as a symmetry-breaking hydrodynamic instability, the rotation taking the place of rectilinear ‘flight.’

Detailed studies of the fluid motion revealed the physical basis for this instability. At low frequencies the motion of the wing produced symmetric paired eddies

from its edges; see Figure 4.1(a). These move away from the wing and have little effect on it. At higher frequencies the eddies become more tightly bound to the wing and can strongly interact with it when the wing is in “flight” and the eddies are carried by the wind. Thus it becomes possible for small vertical movements of the wing to produce thrust, which can sustain the horizontal motion.

Numerical simulations in two dimensions of this bifurcation to forward flight were subsequently carried out by Alben and Shelley [4]. In these computations the wing was an ellipse of a certain density relative to the fluid, which was driven in vertical flapping motion but allowed to move horizontally according to Newton’s laws. Frictional contributions from the bearings, a feature in the physical experiments, were not present. This may explain why no hysteresis or bistability was found in the simulated system. These studies did reveal a bifurcation with a rich structure. Flight was not necessarily initiated by an abrupt acceleration to terminal speed. Oscillations in the horizontal motion, both periodic and chaotic, could also occur and with rising frequency preceded steady forward flight. In fact, the structure of the bifurcation, involving the full force of the Navier-Stokes nonlinearity in a time-dependent flow, has still not been fully elucidated.

We have considered yet more complicated wing-fluid systems. For example, the thrust provided by flapping can be increased by allowing the wing to *pitch* about the horizontal plane. In a combined experimental and numerical study (Spagnolie et al. [42]) we studied a wing equipped with a torsional spring that allowed pitching to occur passively. In this system the symmetry of the rigid wing is broken at any Reynolds number, and while we found a continuous transition to flight through the Stokesian regime, it was only at intermediate Reynolds numbers that flight performance improved rapidly. This study also revealed limits on the improvements due to passive pitching; at sufficiently high  $Re_f$ , wing speed peaks and declines and can actually lead to backwards flight and bistability.

## 4.2 Hovering in an Oscillating Airflow

While hovering is not, strictly speaking, locomotion through a fluid, the mechanisms of lift generation needed to hover are very similar to those for thrust generation. The hovering of birds and insects involves a variety of wing movements and mechanisms for lift enhancement. The key elements are the vortices shed from the edges of the wing during the various phases of the stroke cycle and the movements of the wings through the field of already shed vortices.

In natural hovering the wings are moved actively by the organism. Because of the difficulty of constructing active hoverers for experimental studies, we decided to look at the possibility of the hovering of a body subjected passively to an oscillating airflow. The experimental device that emerged is shown in Figure 4.2. A large speaker drives an oscillating column of air at frequencies in the range 10–40 Hz. We place our “bug” in the test chamber, then increase the amplitude or frequency of the oscillation until hovering occurs. One example of a flexible bug, hovering up and down on a wire, is shown in Figure 4.2 (upper right). This bug was

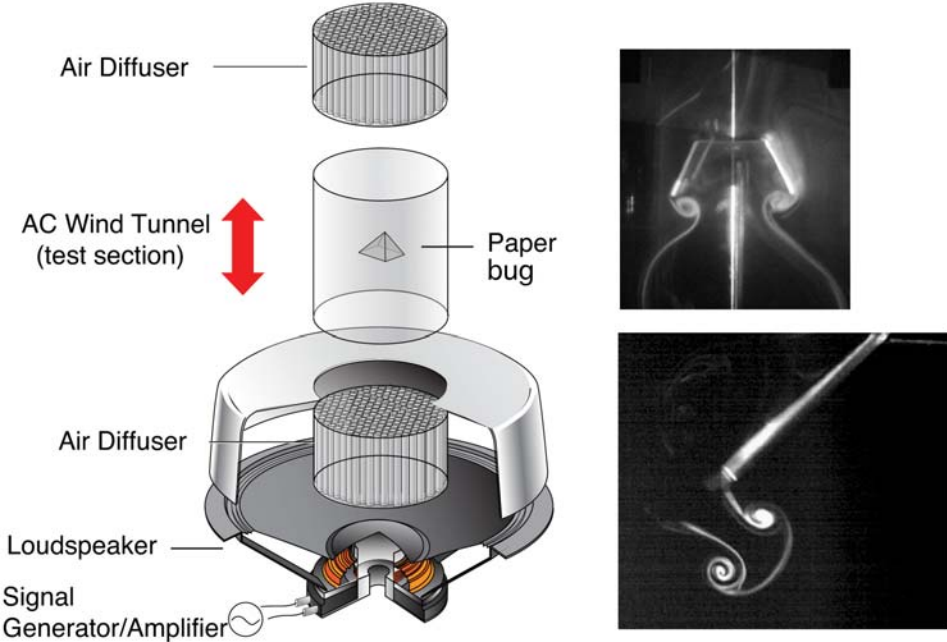


FIGURE 4.2. Left: Device for generating an oscillating airflow. A large loudspeaker drives air through a diffuser and into a cylindrical chamber, creating an AC wind tunnel. Top right: Smoke visualization of the flow around a hovering “paper bug” that is constrained to slide along a vertical wire. Bottom right: A two-dimensional vortex dipole is shed from the edge of a flapping wing. Reproduced from [11, 53] with permission of the authors.

made from folded tissue paper stiffened with lacquer and is 2–5 cm in diameter. High-speed movies of the hovering show that the wings flex in a regular pattern similar to active beating. By constructing geometrically similar bugs of various sizes, we find that for each size there is a unique frequency  $f^*$  at which a bug can hover with minimum amplitude  $A^*$  (maximum-to-minimum excursion of the air in one cycle) of the oscillating flow, with  $f^* A^*$  being roughly independent of size (and approximately 50 cm/s). Also,  $f^*$  increases with decreasing bug size, in a way similar to the increase of beat frequency with decreasing size observed among insects [11].

We were able to model our results qualitatively using a two-dimensional flapping model. This and other experimental studies led to an understanding of the basic mechanism of lift production, which resembles that available in active flapping and hovering. Oscillatory motion of air past a sharp edge tends to produce a pair of oppositely oriented eddies, forming a “vortex dipole”; see Figure 4.2 (lower right). If, for example, the counterclockwise eddy is on the right of the clockwise eddy, then each is advected downward by its neighbor, resulting in the propagation of

the pair as a coherent vortex dipole. (In the case of our three-dimensional bug, the edges of all four side-wings produce structures that combine into a sort of toroidal vortex dipole.) As the dipole propagates downward, it carries momentum. The production of this downward momentum with each flap of the wings is, according to Newton's laws, associated with an upward force on the body that balances its weight. A similar mechanism involving symmetrical bodies that change their shape was also investigated through Navier-Stokes simulations in two dimensions; see Spagnolie and Shelley [43].

We crudely estimate this force as follows: the total circulation  $\Gamma$  (or vortex tube strength) introduced by the upward or downward air motion past an edge in optimal hovering is approximately  $\Gamma \sim f^* A^* \times A^*/2$ . The dipole can be estimated to move at a speed  $U \sim 4\Gamma/a$ , where  $a$  is the radius of the disc of paper forming the bug; we estimate the radius of the cross section of the dipole pair as  $a/4$ , and the length of the dipole tube as  $4a$ . The momentum  $M$  thus produced in one cycle is about  $U$  times twice the virtual mass of a cylinder of radius  $a/4$  in air and the length of tube. Thus  $M \sim (2f^* A^{*2}/a) \times 2\pi(a/4)^2 \rho \times 4a$ , where  $\rho$  is the air density. The rate of momentum transport is  $f^* M \sim \pi\rho(f^* A^* a)^2$ , which must equal  $gm$  where  $m$  is the mass of the bug. Thus  $m \sim \pi\rho(f^* A^* a)^2/g \approx 3\pi a^2$  mg,  $a$  measured in centimeters, given that  $f^* A^* \sim 50$  in optimal hovering. Since our tissue material has a density of  $2.8$  mg/cm<sup>2</sup>, we have reasonable agreement with this estimate. It is interesting that the lift mechanism scales as length squared. For our paper bugs the weight scales similarly, but in general a complex flapping device should have weight scaling as length cubed. This raises the prospect of extremely small active hoverers that nevertheless maintain a sufficiently large Reynolds number to effect the mechanisms studied here.

Following our work with these flexible hoverers, we investigated the possibility that passive hovering could be accomplished with a rigid object. We therefore constructed rigid pyramid-shaped bodies from tissue paper applied to a carbon fiber frame. To our surprise we found that the rigid bodies hovered under similar conditions, presumably by a similar mechanism; see Weathers et al. [53]. Dealing with a rigid body allowed us to interpret the lift as the difference between the "drag" on the object as the air moves downward over it compared to that obtained when the air moves upwards.

One very surprising observation arising from these studies is the stability of hovering. When the pyramidal bodies are dropped in still air, from any initial orientation, they quickly assume an inverted orientation because of their shape and center of gravity. However, in an oscillating airflow the upright "unstable" orientation is in fact quite stable. In ongoing work, we are beginning to understand the cause of this stability; see Liu et al. [26]. It promises to be important in the construction of active hoverers utilizing the mechanisms accessible to study in an oscillating airflow.

### 4.3 A Complementary Problem: Pumping

Locomotion involves interactions of a body with the fluid through which it moves. In a similar way, pumping involves the interactions of a fluid with the boundary of the conduit through which it moves. While the impeller of a mechanical pump is very similar to the propeller of an airplane, pumping also involves other tricks such as the use of valves and centrifugal pressures. Our work in the AML has dealt with a far simpler mechanism known as *valveless pumping*. There are various types of valveless pumps, but all involve moving the walls of a simple conduit, usually a tube. The purpose of the pump may be to move the fluid from one reservoir to another, or it may be to move fluid along a tube despite viscous friction. Probably the most familiar valveless pump is the *peristaltic* pump, where a wave of contraction moves down a flexible tube. In the extreme case the tube closes off at the restrictions and thus carries a bolus of fluid along as if on a conveyor belt. Swallowing of food or drink provides a good example of peristaltic pumping.

The device we examined experimentally is more subtle in its interactions between boundaries and fluid. It utilizes a tube that closes on itself, i.e., a thin toroidal container filled with fluid. Most of the tube is a rigid cylinder, but a small segment is elastic and can be deformed. To induce pumping through this system, the elastic segment is squeezed periodically at an off-center point. Surprisingly fast flows can be built up in this way, by adjustment of the squeezing frequency. The asymmetric placement of the point of squeezing is crucial to the mechanism and to determining the direction of the mean flow. Such a valveless pump is of interest because of its simple construction and because its mechanism may be in operation in animal hearts during early development [15].

An experiment on valveless pumping of this kind was carried out in our lab by graduate student Tom Bringley, who also devised an elegant ODE model of the process [8]. The model accounts for most of the observed properties of valveless pumping. The process is subtle because the interaction of flux, pressure, and wall elasticity occurs not only quasi-steadily but also dynamically through the propagation of hydroelastic waves on the flexible portion of the tube. Bringley's model assumes that the time of transit of these waves is short compared to the time interval between squeezes of the tube. It cannot therefore account for certain resonances associated directly with wave propagation but is effective over most of the parameter range of interest. In earlier work, two-dimensional numerical simulations utilizing the immersed boundary method revealed how these wave interactions can lead to surprising effects, such as flow reversal under a change of frequency [20].

## 5 Current Directions and Future Outlook

Fluid-structure interactions between flexible and/or movable bodies with inertial flows has been a primary and fruitful focus of the AML. This area is of course rich

in phenomenology that is central to answering basic questions in biology, engineering, and geophysics. In moving forward we are particularly interested in devising experiments and theory for fluid-mediated collective behavior of swimming and flying organisms. In one foray into collective dynamics we are studying synthetic nanomotors whose motion is induced by chemical reactions [30]. Synthetic systems have the advantage of removing behavior and internal stochasticity from the study, but often involve fairly complicated physical and chemical processes that are not yet well understood and which can have their own nonbiological quirks (such as the production of electric fields). Outside of the small length-scale regime governed by the Stokes equations, it remains a formidable challenge to construct controlled experiments of freely moving and interacting bodies. The experiments using arrays of flags [33] are a step in this direction in that the body is free to deform itself, though of course its position in the flow relative to the other bodies is fixed. This means of course that typically the flags are producers of drag and not thrust, which affects the nature of the surrounding fluid flows.

There are several recent or ongoing experiments in the AML that investigate the dynamics of complex fluids, which present an extreme version of fluid-structure interactions. In one very recent experiment, we investigated the force transmission properties of “wet” granular media, here an aqueous solution of cornstarch particles at high volume concentration. It is well known that a dry packing of grains transmits an applied force through sparsely distributed and branching force chains. On the other hand, through a normal viscous fluid, a force can be delivered rather uniformly towards the other side of the fluid. The situation with a suspension of grains is much less investigated and has surprising results.

In our experiment a solid sphere is driven slowly through a shear-thickening cornstarch solution; see Figure 5.1 from Liu, Shelley, and Zhang [28] (with permission). We found that the granular fluid dynamically hardens into a solid-like body attached to the sphere, and that this solid can be used to deliver a focused force. The hardened region melts upon cessation of the body’s motion. We investigated the scaling and geometric form of the hardened mass with sphere size and speed (actually suspension strain rate), and its dependence upon the shape of the penetrating body. This work demonstrated how stress hardening of fluidic materials can be used to assemble temporary and useful structures and gives another route to force transmission that lies somewhere between solids (elastic and plastic deformation) and fluid (strain-rate modulated dissipation).

Another ongoing experiment involves a layer of fluid that overlays an array of disks that rotate and counterrotate to set up an array of vortices and hyperbolic stagnation points. This experiment investigates the onset of symmetry breaking bifurcations and flow oscillations that were predicted from theoretical studies of Shelley and his collaborators, particularly B. Thomases [47, 48, 49]. A second experiment involves a body moving in a viscoelastic fluid while under an oscillatory body force. The point of this experiment is to investigate the interaction of two timescales, that of the fluid “relaxation time,” which is intrinsic to a viscoelastic

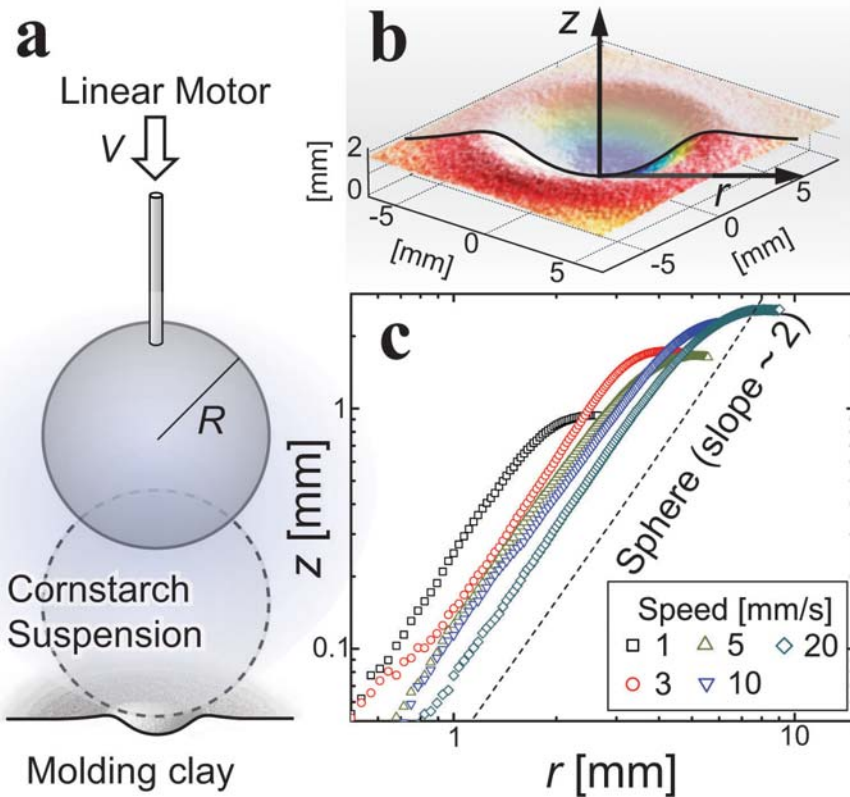


FIGURE 5.1. A sphere moves slowly through a suspension of cornstarch, causing a focused depression on a flat layer of molding clay. (a) The depression is created by a sphere of radius  $R = 12.7$  mm, which is driven downward by a linear motor. The sphere stops short of the clay surface, at  $H = 0$ . (b) The shape of the depression is digitized and shown as its elevation  $z$  against radius  $r$ . (c) Each profile created at a different impact speed suggests a parabolic shape. The slower the impact speed, the larger the indent curvature. The dashed line shows the corresponding profile of the sphere that caused all depressions. Reproduced from [28] with permission of the authors.

fluid, and that of the forcing. Recent numerical experiments investigating sperm motility in a viscoelastic fluid have suggested that locomotion is enhanced when these two timescales are comparable; see Teran, Fauci, and Shelley [46].

Finally, as mentioned above, new experiments are involving synthetic microswimmers that are composed of bimetallic rods, gold and platinum, that move through two catalytic reactions with hydrogen peroxide to produce a directed proton flow along its surface. With this system we hope to investigate many-body interactions experimentally, as has been done in biological systems using bacteria

(see, for example, Dombrowski et al. [14]), as well as how microswimmers interact with complex geometries.

This work is related, again, to theoretical work on many-swimmer suspensions by Shelley and his collaborators D. Saintillan and C. Hohenegger [18, 35, 36, 37, 38]. In that work, collective behavior was modeled using tools developed for complex fluids where Fokker-Planck equations for evolving the motile particle conformation distribution function are coupled to the flows produced by the collective motion. This has been very successful in the Stokesian regime, where such theories make testable predictions, such as changes in stability with swimmer concentration. Little has been done in this direction in higher-speed flows due to the complications of efficiently modeling locomotory mechanisms, vorticity production, and turbulent dissipation.

As the above work on suspensions and microswimmers suggests, the AML has been moving towards the small. Developmental biology brings a whole host of new fluid-structure interaction problems such as how nuclei are moved about within the cell [41], or how mitotic spindles are formed in the approach to cell division. The important biological components—microtubules, actin, motor proteins, ATP/ADP—could be elements of future “smart fluids” that are engineered to perform technological tasks.

There are also other interesting fluid-structure problems that arise in geophysics and which in some reduced form might be amenable to experimentation. One example is pattern formation through fluid erosion. While these are difficult free-boundary problems, they are somewhat simplified by the separation of flow time-scales from erosion timescales. Also, clays and muds can have plastic responses beyond a critical yield stress. A very different and interesting class of problems at a far larger scale concerns how suspended objects aggregate in a fluid, and how these aggregates may affect the circulation of fluid and other processes such as heat absorption and transfer. The problem that comes to mind is understanding the appearance and effect of vast aggregates of plastic particulates in the Earth’s oceans (e.g., the “Great Pacific Garbage Patch”).

To close, we find that a physical laboratory can be a stimulating and vibrant part of an applied mathematics environment. An important part of this are experiments that are simple enough that the kernel of a physical interaction can be revealed. Such experiments in the AML have provoked new mathematical modeling and analysis, and the development of new numerical methods that address fundamental problems in fluid-structure interaction. We have also found that theorists can develop an “experimental intuition” that also allows them to contribute to the course of experiment. From our experience the AML has become a true interdisciplinary platform where scientists from many different backgrounds—mathematics, physics, biology, chemistry—can work together.

**Acknowledgment.** We gratefully acknowledge the William Sears family for their bequest to NYU, and to the Zegar Foundation and the Lilian and George Lytle Chair in Applied Mathematics for their continuing support of the AML. We gratefully acknowledge grant support from the Department of Energy and the National Science Foundation. We would also like to acknowledge the many excellent postdocs and students who have come through the lab and contributed to its success through their imaginative research. Lastly, we would like to thank Albert Libchaber for his early and continuing encouragement and advice.

## Bibliography

- [1] Alben, S. The flapping-flag instability as a nonlinear eigenvalue problem. *Phys. Fluids* **20** (2008), no. 10, 104106, 11pp. doi:10.1063/1.3000670
- [2] Alben, S. Simulating the dynamics of flexible bodies and vortex sheets. *J. Comput. Phys.* **228** (2009), no. 7, 2587–2603. doi:10.1016/j.jcp.2008.12.020
- [3] Alben, S. Wake-mediated synchronization and drafting in coupled flags. *J. Fluid Mech.* **641** (2009), 489–496. doi:10.1017/S0022112009992138
- [4] Alben, S.; Shelley, M. Coherent locomotion as an attracting state for a free flapping body. *Proc. Nat. Acad. Sci. (USA)* **102** (2005), no. 32, 11163–11166. doi:10.1073/pnas.0505064102
- [5] Alben, S.; Shelley, M. Flapping states of a flag in an inviscid fluid: bistability and the transition to chaos. *Phys. Rev. Lett.* **100** (2008), no. 7, 074301, 4pp. doi:10.1103/PhysRevLett.100.074301
- [6] Alben, S.; Shelley, M.; Zhang, J. Drag reduction through self-similar bending of a flexible body. *Nature* **420** (2002), 479–481. doi:10.1038/nature01232
- [7] Alben, S.; Shelley, M.; Zhang, J. How flexibility induces streamlining in a two-dimensional flow. *Phys. Fluids* **16** (2004), 1694–1713. doi:10.1063/1.1668671
- [8] Bringley, T. T.; Childress, S.; Vandenbergh, N.; Zhang, J. An experimental investigation and a simple model of a valveless pump. *Phys. Fluids* **20** (2008), 033602, 15pp. doi:10.1063/1.2890790
- [9] Childress, S. Eulerian mean flow from an instability of convective plumes. *Chaos* **10** (2000), no. 1, 28–38. doi:10.1063/1.166473
- [10] Childress, S.; Dudley, R. Transition from ciliary to flapping mode in a swimming mollusc: flapping flight as a bifurcation in  $Re_\omega$ . *J. Fluid Mech.* **498** (2004), 257–288. doi:10.1017/S002211200300689X
- [11] Childress, S.; Vandenbergh, N.; Zhang, J. Hovering of a passive body in an oscillating airflow. *Phys. Fluids* **18** (2006), 117103, 9pp. doi:10.1063/1.2371123
- [12] Couder, Y.; Chomaz, J. M.; Rabaud, M. On the hydrodynamics of soap films. *Physica D* **37** (1989), no. 1–3, 384–405. doi:10.1016/0167-2789(89)90144-9
- [13] Denny, M. Extreme drag forces and the survival of wind-swept and water-swept organisms. *J. Exp. Bio.* **194** (1994), 97–115.
- [14] Dombrowski, C.; Cisneros, L.; Chatkaew, S.; Goldstein, R. E.; Kessler, J. O. Self-concentration and large-scale coherence in bacterial dynamics. *Phys. Rev. Lett.* **93** (2004), 098103, 4pp. doi:10.1103/PhysRevLett.93.098103
- [15] Forouhar, A. S.; Liebling, M.; Hickerson, A.; Nasiraei-Moghaddam, A.; Tsai, H.-J.; Hove, J. R.; Fraser, S. E.; Dickinson, M. E.; Gharib, M. The embryonic vertebrate heart tube is a dynamic suction pump. *Science* **312** (2006), no. 5774, 751–753. doi:10.1126/science.1123775
- [16] Gharib, M.; Derango, P. A liquid-film (soap film) tunnel to study two-dimensional laminar and turbulent shear flows. *Physica D* **37** (1989), no. 1–3, 406–416. doi:10.1016/0167-2789(89)90145-0
- [17] Helmholtz, H. Über discontinuierliche flüssigkeitsbewegungen. *Monatsber. Berlin Akad.* **23** (1868), 215–228.

- [18] Hohenegger, C.; Shelley, M. J. Stability of active suspensions. *Phys. Rev. E (3)* **81** (2010), no. 4, 046311, 10pp. doi:10.1103/PhysRevE.81.046311
- [19] Hureau, J.; Brunon, E.; Legallais, Ph. Ideal free streamline flow over a curved obstacle. *J. Comput. Appl. Math.* **72** (1996), no. 1, 193–214. doi:10.1016/0377-0427(95)00272-3
- [20] Jung, E.; Peskin, C. S. Two-dimensional simulations of valveless pumping using the immersed boundary method. *SIAM J. Sci. Comput.* **23** (2001), no. 1, 19–45. doi:10.1137/S1064827500366094
- [21] Jung, S.; Mareck, K.; Shelley, M.; Zhang, J. Dynamics of a deformable body in a fast flowing soap film. *Phys. Rev. Lett.* **97** (2006), no. 13, 134502, 4pp. doi:10.1103/PhysRevLett.97.134502
- [22] Kim, Y.; Peskin, C. S. Penalty immersed boundary method for an elastic boundary with mass. *Phys. Fluids* **19** (2007), no. 5, 053103, 18pp. doi:10.1063/1.2734674
- [23] Koehl, M. A. R. How do benthic organisms withstand moving water? *Amer. Zool.* **24** (1984), no. 1, 57–70. doi:10.1093/icb/24.1.57
- [24] Koehl, M. A. R. When does morphology matter? *Annu. Rev. Ecol. Syst.* **27** (1996), 501–542. doi:10.1146/annurev.ecolsys.27.1.501
- [25] Liao, J. C.; Beal, D. N.; Lauder, G. V.; Triantafyllou, M. S. Fish exploiting vortices decrease muscle activity. *Science* **302** (2003), no. 5650, 1566–1569. doi:10.1126/science.1088295
- [26] Liu, B.; Ristroph, L.; Weathers, A.; Childress, S.; Zhang, J. Intrinsic stability of a body hovering in an oscillating airflow. *Phys. Rev. Lett.* **108** (2012), no. 6, 068103, 5pp. doi:10.1103/PhysRevLett.108.068103
- [27] Liu, B.; Zhang, J. Self-induced cyclic reorganization of many bodies through thermal convection. *Phys. Rev. Lett.* **100** (2008), no. 24, 244501, 4pp. doi:10.1103/PhysRevLett.100.244501
- [28] Liu, B.; Shelley, M.; Zhang, J. Focused force transmission through an aqueous suspension of granules. *Phys. Rev. Lett.* **105** (2010), no. 18, 188301, 4pp. doi:10.1103/PhysRevLett.105.188301
- [29] Niklas, K. J. The influence of gravity and wind on land plant evolution. *Rev. Palaeobot. Palyno.* **102** (1998), no. 1–2, 1–14. doi:10.1016/S0034-6667(98)00011-6
- [30] Paxton, W. F.; Kistler, K. C.; Olmeda, C. C.; Sen, A.; St. Angelo, S. K.; Cao, Y.; Mallouk, T. E.; Lammert, P. E.; Crespi, V. H. Catalytic nanomotors: Autonomous movement of striped nanorods. *J. Am. Chem. Soc.* **126** (2004), no. 1, 13424–13431. doi:10.1021/ja047697z
- [31] Purcell, E. M. Life at low Reynolds numbers. *Am. J. Phys.* **45** (1997), no. 1, 3–11. doi:10.1119/1.10903
- [32] Rayleigh, L. On the instability of jets. *Proc. London Math. Soc.* **s1-10** (1878), no. 1, 4–13. doi:10.1112/plms/s1-10.1.4
- [33] Ristroph, L.; Zhang, J. Anomalous hydrodynamical drafting of interacting flapping flags. *Phys. Rev. Lett.* **101** (2008), 194502, 4pp. doi:10.1103/PhysRevLett.101.194502
- [34] Rutgers, M. A.; Wu, X. L.; Daniel, W. B. Conducting fluid dynamics experiments with vertically falling soap films. *Rev. Sci. Instrum.* **72** (2001), no. 7, 3025–3037. doi:10.1063/1.1379956
- [35] Saintillan, D.; Shelley, M. Orientational order and instabilities in suspensions of self-locomoting rods. *Phys. Rev. Lett.* **99** (2007), no. 5, 058102, 4pp. doi:10.1103/PhysRevLett.99.058102
- [36] Saintillan, D.; Shelley, M. J. Instabilities and pattern formation in active particle suspensions: kinetic theory and continuum simulations. *Phys. Rev. Lett.* **100** (2008), no. 17, 178103, 4pp. doi:10.1103/PhysRevLett.100.178103
- [37] Saintillan, D.; Shelley, M. J. Instabilities, pattern formation and mixing in active suspensions. *Phys. Fluids* **20** (2008), no. 12, 123304, 16pp. doi:10.1063/1.3041776
- [38] Saintillan, D.; Shelley, M. J. Emergence of coherent structures and large-scale flows in motile suspensions. *J. R. Soc. Interface* **9** (2011), no. 68, 571–585.
- [39] Shelley, M.; Vandenberghe, N.; Zhang, J. Heavy flags undergo spontaneous oscillations in flowing water. *Phys. Rev. Lett.* **94** (2005), no. 9, 094302, 4pp. doi:10.1103/PhysRevLett.94.094302

- [40] Shelley, M. J.; Zhang, J. Flapping and bending bodies interacting with fluid flows. *Annu. Rev. Fluid Mech.* **43** (2011), 449–465. doi:10.1146/annurev-fluid-121108-145456
- [41] Shinar, T.; Mano, M.; Piano, F.; Shelley, M. J. A model of cytoplasmically-driven microtubule-based motion in the single-celled *Caenorhabditis elegans* embryo. *Proc. Natl. Acad. Sci. USA* **108** (2011), no. 26, 10508–10513. doi:10.1073/pnas.1017369108
- [42] Spagnolie, S. E.; Moret, L.; Shelley, M. J.; Zhang, J. Surprising behaviors in flapping locomotion with passive pitching. *Phys. Fluids* **22** (2010), no. 4, 041903, 20pp. doi:10.1063/1.3383215
- [43] Spagnolie, S. E.; Shelley, M. J. Shape-changing bodies in fluid: hovering, ratcheting, and bursting. *Phys. Fluids* **21** (2009), no. 1, 013103, 13pp. doi:10.1063/1.3054143
- [44] Stewart, H. L. Hydrodynamic consequences of flexural stiffness and buoyancy for seaweeds: a study using physical models. *J. Exp. Bio.* **209** (2006), 2170–2181. doi:10.1242/jeb.02254
- [45] Taylor, G. I. Low Reynolds number flows. National Committee for Fluid Mechanics Films, 1967. Available at: [http://modular.mit.edu:8080/ramgen/ifluids/Low\\_Reynolds\\_Number\\_Flow.rm](http://modular.mit.edu:8080/ramgen/ifluids/Low_Reynolds_Number_Flow.rm)
- [46] Teran, J.; Fauci, L.; Shelley, M. Viscoelastic fluid response can increase the speed and efficiency of a free swimmer. *Phys. Rev. Lett.* **104** (2010), no. 3, 038101, 4pp. doi:10.1103/PhysRevLett.104.038101
- [47] Thomas, B.; Shelley, M. Emergence of singular structures in Oldroyd-b fluids. *Phys. Fluids* **19** (2007), no. 10, 103103, 12pp. doi:10.1063/1.2783426
- [48] Thomas, B.; Shelley, M. Transition to mixing and oscillations in a Stokesian viscoelastic flow. *Phys. Rev. Lett.* **103** (2009), no. 9, 094501, 4pp. doi:10.1103/PhysRevLett.103.094501
- [49] Thomas, B.; Shelley, M.; Thiffeault, J.-L. A Stokesian viscoelastic flow: Transition to mixing and oscillations. *Physica D* **240** (2011), no. 20, 1602–1614. doi:10.1016/j.physd.2011.06.011
- [50] Vandenbergh, N.; Childress, S.; Zhang, J. On unidirectional flight of a free flapping wing. *Phys. Fluids* **18** (2006), no. 1, 014102, 8pp. doi:10.1063/1.2148989
- [51] Vandenbergh, N.; Zhang, J.; Childress, S. Symmetry breaking leads to forward flapping flight. *J. Fluid Mech.* **506** (2004), 147–155. doi:10.1017/S0022112004008468
- [52] Vogel, S. Drag and reconfiguration of broad leaves in high winds. *J. Exp. Bot.* **40** (1989), no. 8, 941–948. doi:10.1093/jxb/40.8.941
- [53] Weathers, A.; Folie, B.; Liu, B.; Childress, S.; Zhang, J. Hovering of a rigid pyramid in an oscillatory airflow. *J. Fluid Mech.* **650** (2010), 415–425. doi:10.1017/S0022112010000583
- [54] Weihs, D. Hydromechanics of fish schooling. *Nature* **241** (1973), 290–291. doi:10.1038/241290a0
- [55] Zhang, J.; Childress, S.; Libchaber, A. Non-Boussinesq effect: thermal convection with broken symmetry. *Phys. Fluids* **9** (1997), no. 4, 1034–1042. doi:10.1063/1.869198
- [56] Zhang, J.; Childress, S.; Libchaber, A. Non-Boussinesq effect: asymmetric velocity profiles in thermal convection. *Phys. Fluids* **10** (1998), no. 6, 1534–1536. doi:10.1063/1.869672
- [57] Zhang, J.; Childress, S.; Libchaber, A.; Shelley, M. Flexible filaments in a flowing soap film as a model for one-dimensional flags in a two-dimensional wind. *Nature* **408** (2000), 835–839. doi:10.1038/35048530
- [58] Zhang, J.; Libchaber, A. Periodic boundary motion in thermal turbulence. *Phys. Rev. Lett.* **84** (2000), no. 19, 4361–4364. doi:10.1103/PhysRevLett.84.4361
- [59] Zhong, J.-Q.; Zhang, J. Thermal convection with a freely moving top boundary. *Phys. Fluids* **17** (2005), no. 11, 115105, 12pp. doi:10.1063/1.2131924
- [60] Zhu, L.; Peskin, C. S. Interaction of two flapping filaments in a flowing soap-film. *Phys. Fluids* **15** (2003), no. 7, 1954–1960. doi:10.1063/1.1582476
- [61] Zhu, L.; Peskin, C. S. Simulation of a flapping flexible filament in a flowing soap film by the immersed boundary method. *J. Comput. Phys.* **179** (2002), no. 2, 452–468. doi:10.1006/jcph.2002.7066

STEPHEN CHILDRESS  
Courant Institute  
251 Mercer St., Rm. 1305  
New York, NY 10012  
E-mail: [childress@cims.nyu.edu](mailto:childress@cims.nyu.edu)

MICHAEL SHELLEY  
Courant Institute  
251 Mercer St., Rm. 1102  
New York, NY 10012  
E-mail: [shelley@cims.nyu.edu](mailto:shelley@cims.nyu.edu)

JUN ZHANG  
Courant Institute  
251 Mercer St., Rm. 1118  
New York, NY 10012  
E-mail: [jun@cims.nyu.edu](mailto:jun@cims.nyu.edu)

Received October 2011.